ACS NANO

www.acsnano.org

ARTICLE

Omnidirectionally Stretchable and Transparent Graphene Electrodes

Jin-Yong Hong,[†,‡] Wook Kim,[§] Dukhyun Choi,[§] Jing Kong,[*,‡] and Ho Seok Park[*,†]

[†]School of Chemical Engineering, Sungkyunkwan University, Suwon 440-746, Korea

[‡]Department of Electrical Engineering and Computer Science, Massachusetts Institute of Technology, 77 Massachusetts Avenue, Cambridge, Massachusetts 02139, United States

[§]Department of Mechanical Engineering, Kyung Hee University, 1 Seocheon-dong, Yongin-si, Gyeonggi-do 446-701, Korea

Supporting Information

ABSTRACT: **Stretchable and transparent electrodes have been developed for applications in flexible and wearable electronics. For customer-oriented practical applications, the electrical and optical properties of stretchable electrodes should be independent of the directions of the applied stress, and such electrodes are called omnidirectionally stretchable electrodes. Herein, we report a simple and cost-effective approach for the fabrication of omnidirectionally stretchable and transparent graphene electrodes with mechanical durability and performance reliability. The use of a Fresnel lens-patterned electrode allows multilayered graphene sheets to achieve a concentric circular wavy structure, which is capable of sustaining tensile strains in all directions. The as-prepared electrodes exhibit high optical transparency, low sheet resistance, and reliable electrical performances under various deformation (*e.g.*, bending, stretching, folding, and buckling) conditions. Furthermore, computer simulations have also been carried out to investigate the response of a Fresnel lens-patterned structure on the application of mechanical stresses. This study can be significant in a large variety of potential applications, ranging from stretchable devices to electronic components in various wearable integrated systems.**

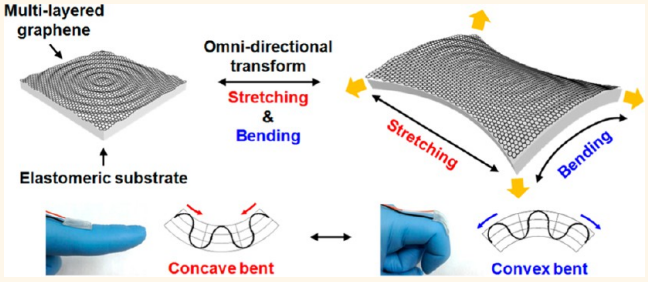

KEYWORDS: *graphene, electrodes, flexible electronics, structure–property relationships*

Stretchable and transparent electrodes have been touted as a key component of the "next generation of electronics".[1−3] These electrodes can be formed into nonplanar forms to make them suitable for applications in flexible and wearable electronics such as rolled-up displays, smart clothing, skin-like sensors, stretchable solar cells, and other easily collapsible gadgets.

Current approaches toward the fabrication of stretchable electrodes can be divided into two categories. One is "materials that stretch", and the other is "structures that stretch". From the viewpoint of materials, the stretchable electrodes are composed of elastomeric matrices (*e.g.*, polydimethylsiloxane (PDMS) and other silicone rubbers) with embedded conductive fillers, such as conducting polymers,[4−6] carbon nanotubes (CNTs),[7−11] metal nanoparticles, and metal nanowires (NWs).[12−15] Stretchability of these electrodes is mainly dominated by the viscoelasticity of the matrix. Despite their good electrical conductivity, the performance of these materials degrades on deformation and they exhibit poor optical properties because of the low transmittance of conductive fillers and the high threshold concentration.

Thus, recent research on stretchable electrodes has been focused on the structure design. From the viewpoint of structure strategy, the conductive materials are assembled into a stretchable architecture, such as wrinkled, buckled, and waved structures, which can be easily stretched.[16−21] Under the applied tensile force, these structures can be stretched and then returned to their original dimension, and thus, the conductive materials can preserve their electrical property in the deformed state. However, most of the existing stretchable electrodes can only be stretched in one direction. For customer-oriented real applications, the electrical and optical properties of stretchable electrodes should be independent of the directions of applied stress; such electrodes are called omnidirectionally stretchable electrodes.

Chemical vapor deposition (CVD)-grown graphene is considered a potential candidate as a stretchable and transparent electrode material because of its low sheet resistance, exceptional mechanical and chemical stabilities, and high optical

Received: July 6, 2016
Accepted: September 29, 2016
Published: September 29, 2016

ACS Publications © 2016 American Chemical Society

DOI: 10.1021/acsnano.6b04493
ACS Nano 2016, 10, 9446−9455

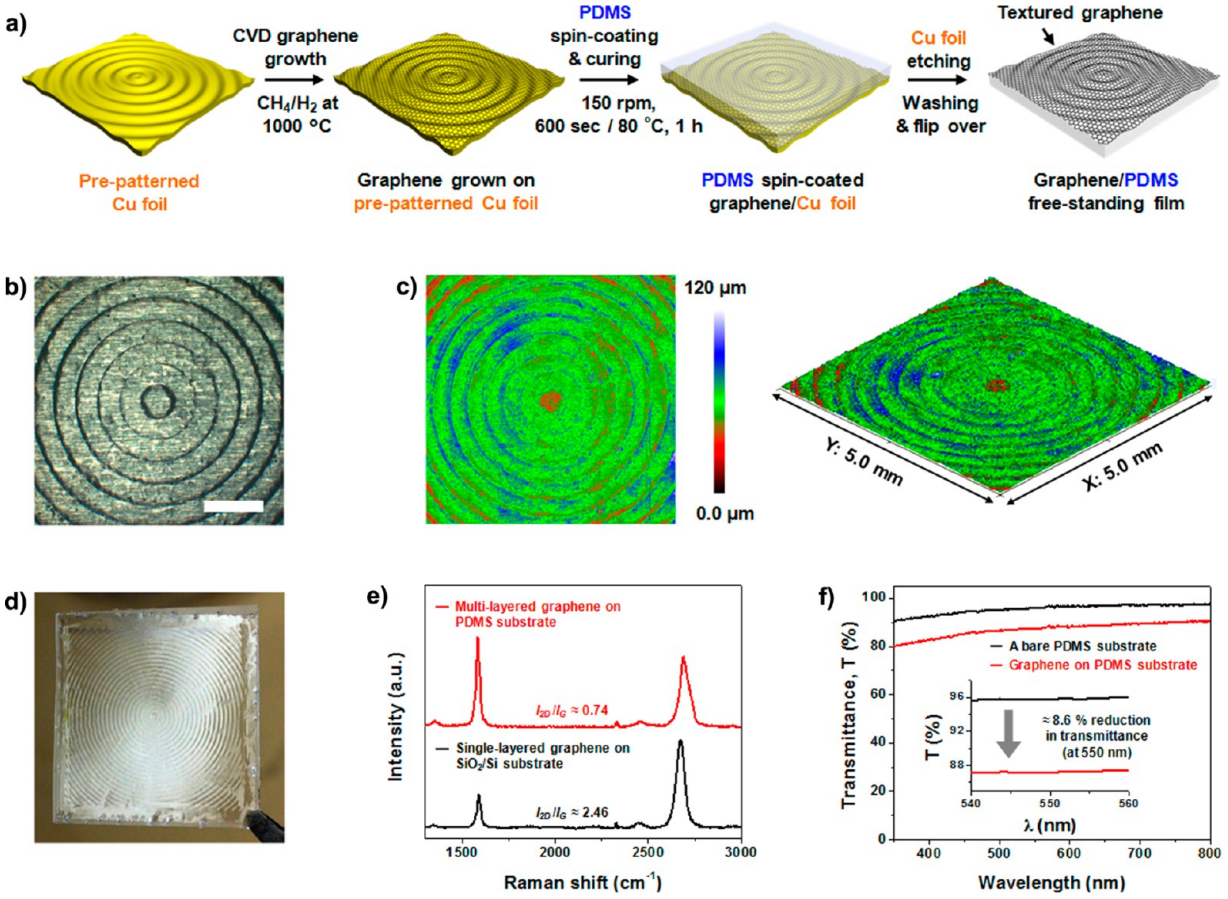

Figure 1. (a) Schematic illustration of the different steps in the fabrication of transparent conductive electrodes including CVD graphene growth, PDMS spin-coating, curing, and Cu etching. (b) Optical microscopy image of graphene/PDMS (scale bar is 1 mm). (c) Three-dimensional topography of a graphene/PDMS film using an α-step profilometer. (d) Photograph of a graphene/PDMS free-standing film. (e) Raman spectra (on excitation with 532 nm) of single-layered graphene (black) and multilayered graphene (red) on a SiO_2/Si substrate. (f) Transmission spectra of a flat PDMS substrate (black) and multilayered graphene on a flat PDMS substrate (red).

transparency.[22−26] Graphene-based electrodes could be made stretchable by combining them with stretchable structures such as a wrinkled multilayer graphene film,[27,28] buckled graphene film,[29] wavy-shaped polyaniline/graphene,[30] and graphene−CNT-layered structure.[31] However, the stretchability is limited by the high stiffness of graphene in two dimensions.[32,33] Although many intensive studies have been carried out on unidirectional stretchable electrodes, to the best of our knowledge, no studies have been reported on solely graphene-based electrodes that show omnidirectional stretchability.

Herein, we report a simple and cost-effective approach for the fabrication of omnidirectionally stretchable and transparent graphene electrodes. This technique allows the multilayered graphene sheets to achieve a concentric circular wavy structure, which is capable of sustaining tensile strains in all directions. The as-prepared electrodes exhibit high optical transparency, low sheet resistance, and reliable electrical performances under various deformation conditions (*e.g.*, bending, stretching, folding, and buckling). Furthermore, computer simulations have also been carried out to investigate the response of the concentric circular wavy structure on the application of mechanical stresses.

RESULTS AND DISCUSSION

The fabrication process of the omnidirectionally stretchable and transparent graphene electrode is illustrated in Figure 1a. Cu foil (99.8%, Alfa Aesar) was prepatterned by pressing it with a Fresnel lens, which acted as a mold. Multilayered graphene was grown on these prepatterned 25 μm thick Cu foils in concentric circle patterns by a typical atmospheric pressure chemical vapor deposition process, as described in previous literature.[34,35] After the growth process, PDMS was coated on the multilayered graphene on the prepatterned Cu foil by spin-coating. The elastomeric PDMS film (around 2.0 mm thick) was thermally cured, and the Cu foil was then chemically etched away by a Cu etchant. Subsequently, the multilayered graphene/PDMS film was rinsed with deionized water and dried at 60 °C for 12 h.

The multilayered graphene/PDMS film was characterized by optical microscopy (OM) and an α-step profilometer, and the results are shown in Figure 1b−d. The OM and photograph images of the multilayered graphene/PDMS film exhibit well-defined, concentric circle patterns. The images also show that the concentric circle pattern of the prepatterned Cu foil remained the same without any smoothing or roughening effects in micrometer scale (see the Supporting Information S1).[36−38] Most of the isotropic ripple (wavy) patterns were preserved throughout the high-temperature CVD process and successfully replicated on the PDMS substrate. In addition, the prepatterned Cu foils can be formed with various shapes (1 × 1,

DOI: 10.1021/acsnano.6b04493
ACS Nano 2016, 10, 9446−9455

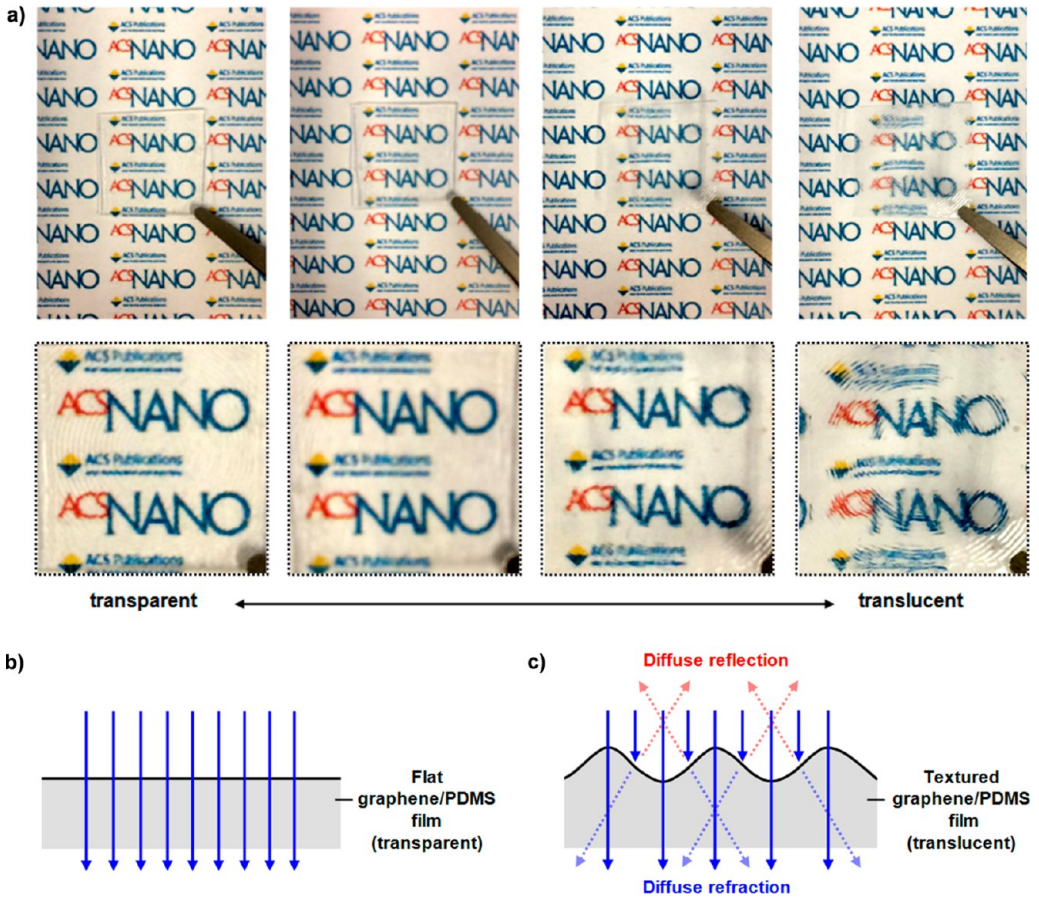

Figure 2. (a) Optical hazing on the textured graphene/PDMS film. Photographs were taken at different distances between the image and the textured graphene/PDMS film. The distances are 0, 0.5, 1.0, and 3.0 cm, respectively. Differences occur between transparency and translucency. The schematic illustration on the (b) left has high transparency, whereas the image on the (c) right has diffuse reflection and has high transparency (translucency).

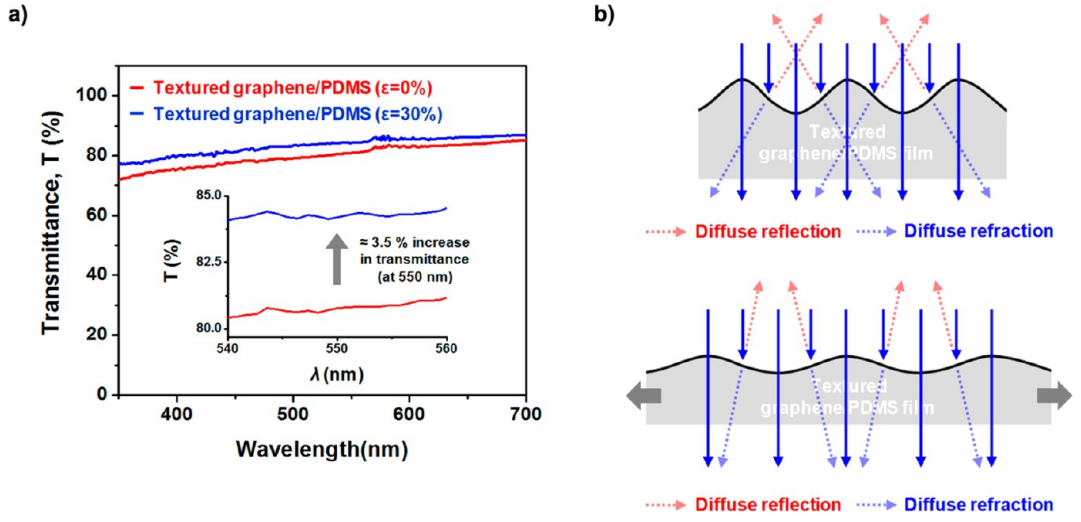

Figure 3. (a) Optical transmittance spectra of textured graphene samples under different tensile strains. (b) Schematic illustration of the transmittance mechanism for textured graphene at 0% and 30% tensile strain.

2 × 2, and 3 × 3 formations) and applied to the articulated section as a joint electrode (see the Supporting Information S2).

Raman spectroscopy was used to investigate the quality of the multilayered graphene on the prepatterned Cu foil using a 532 nm laser excitation. As indicated by the black line in Figure 1e, single-layered graphene on a SiO_2/Si wafer shows a typical monolayer graphene Raman spectrum with two typical G and 2D bands at 1590 and 2675 cm^{-1}, respectively, with a ratio of integrated peak intensities (I_{2D}/I_G) larger than 2.0. The I_{2D}/I_G ratio is known to depend on the number of graphene layers.[39−43] The I_{2D}/I_G ratio in the Raman spectrum of the

DOI: 10.1021/acsnano.6b04493
ACS Nano 2016, 10, 9446−9455

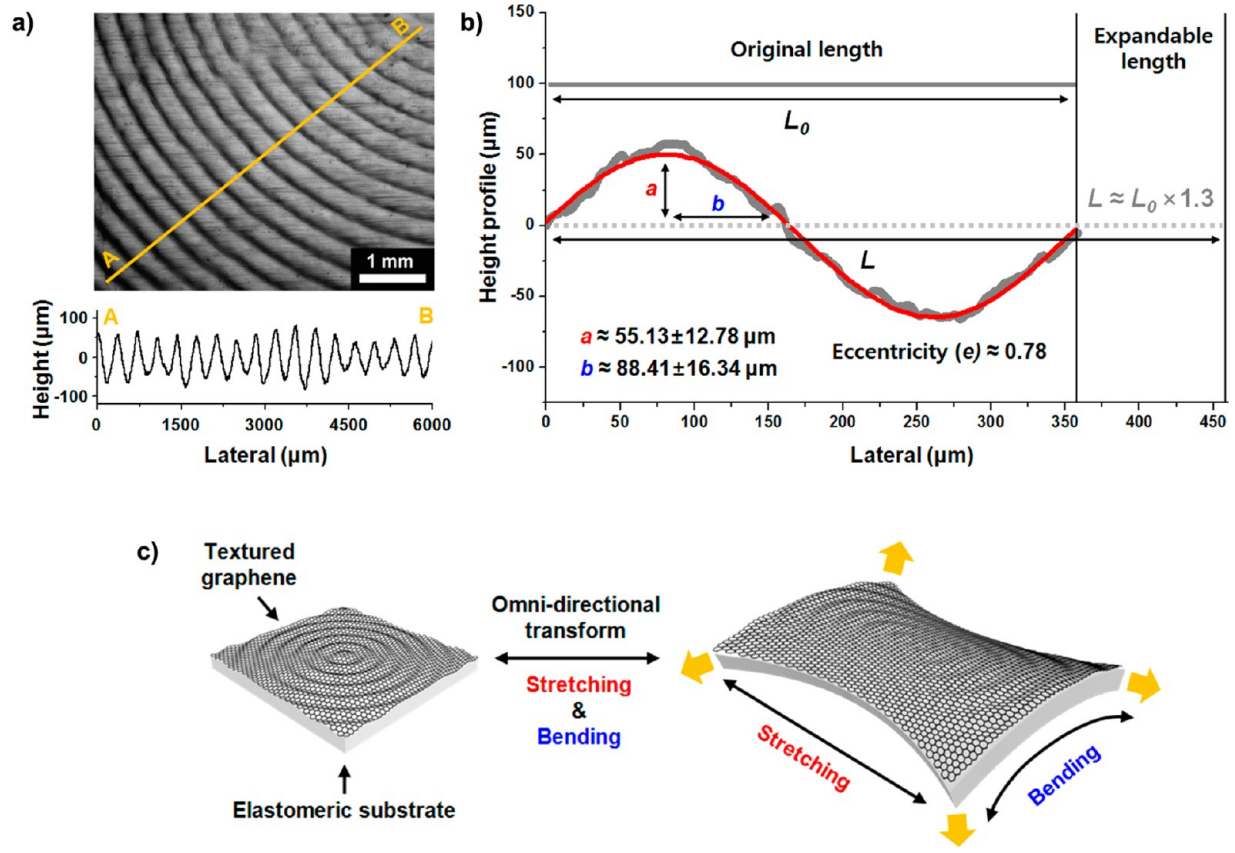

Figure 4. (a) OM image of a graphene/PDMS film with a concentric circle pattern and two-dimensional line scan profile taken vertically through the yellow line on the OM image. (b) Enlarged surface topography of a graphene/PDMS film. Fitting curve is indicated by the red line. (c) Schematic illustration of the transformation of the graphene/PDMS film under applied forces.

graphene samples in the present study is about 0.7, indicating the formation of multilayer graphene.

Optical transmittance was measured to determine the number of layers in the prepared graphene samples, and the results are given in Figure 1f. The multilayered graphene exhibits a transmittance of 87.1% at 550 nm, whereas the bare PDMS substrate has a transmittance of 95.7%, indicating 8.6% loss in transparency due to the graphene. Given that the transmittance reduction by one graphitic layer is approximately 2.3%, the results on the observed transmittance indicate that the average number of layers in the multilayered graphene is about 3 or 4.[44−46] Although multilayered graphene and PDMS has high optical transmittance, the optical transmittance of the textured graphene/PDMS film depends on the distance between the film and the subject.

We are minutely investigating the optical transmittance as a function of distance between an object and the textured graphene/PDMS film (0.0, 0.5, 1.0, and 3.0 cm) (Figure 2a). Corresponding photographs show that the optical transmittance of the textured graphene/PDMS film depends on the distance. For instance, when they stick together, the textured graphene/PDMS film seems transparent. However, as the distance gradually increases, the object seen through the textured graphene/PDMS film becomes blurred (translucent). In general, an object looks transparent when light waves pass through unchanged. The light wave effectively passes through the flat graphene/PDMS film without being dispersed or scattered (Figure 2b). As a result, we can see straight through it, almost as though it is not even there. However, light that strikes uneven surfaces is refracted or reflected, giving a "haze" effect.[47] The haze is caused by a microscopic surface structure that slightly changes the direction of the light (Figure 2c).[48] Likewise, the wrinkle patterns in the textured graphene/PDMS film gave rise to changes in optical transmittance.

Furthermore, to investigate haze effects on the optical properties of textured graphene/PDMS films, we performed UV−vis spectroscopy of the textured graphene/PDMS films at different tensile strains. As shown in Figure 3a, there has been a slight reduction in the transmittance of the textured graphene/PDMS film due to the haze effect (the transmittance of the flat graphene/PDMS film is 87.1% at 550 nm in Figure 1f), and the transmittance of textured graphene slightly increased from 80.7% (at 0% tensile strain) to 84.2% (at 30% tensile strain). This phenomenon can be elucidated by a change in the wavy structure (wavelength and amplitude). As shown in Figure 3b, the applied tensile strain makes the textured surface smoother (or flatter), so that the diffuse reflection/refraction can be diminished. Furthermore, the transmission of incident light becomes more dominant, inducing an increase in transmittance.

Figure 4a shows a top-view OM image of the textured graphene/PDMS film. The OM image clearly shows wavy patterns with concentric circles. The configuration and parameters of the pattern can be more clearly observed in the enlarged image of the height profile. The gray and red curves represent the measured and fitted data, respectively. The height analysis reveals that the average wavelength and amplitude of the pattern are *ca.* 350 and 55 μm, respectively. From the roughly estimated values of the wave pattern

DOI: 10.1021/acsnano.6b04493
ACS Nano 2016, 10, 9446−9455

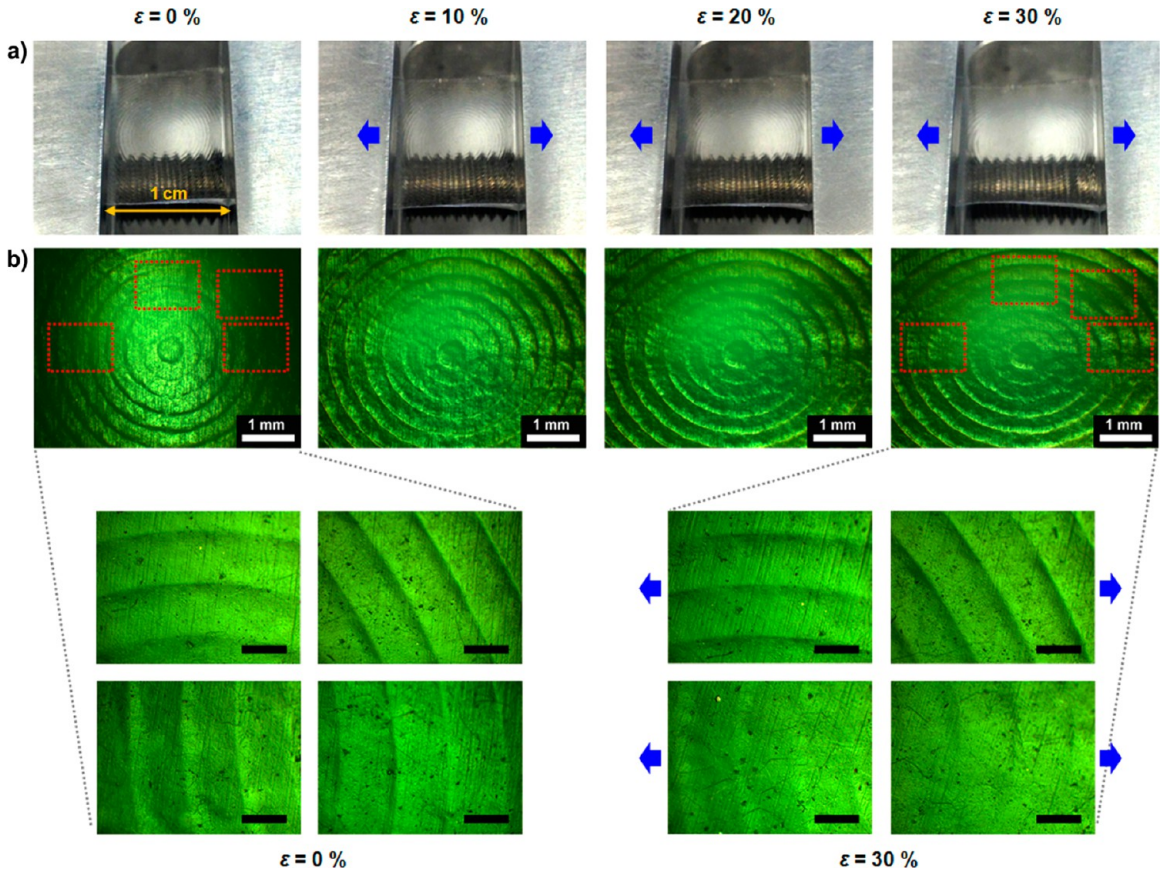

Figure 5. (a) Stretching test images for the textured graphene/PDMS film. Stretching tests were performed under various tensile strains (from 0% to 30%). (b) Corresponding OM images for the textured graphene/PDMS film under various tensile strains. Enlarged optical images were taken at different parts shown in the red boxes (scale bar indicates 200 μm).

parameters, we can approximately calculate the stretchability of the textured graphene/PDMS film under tensile stress. Assuming an elliptical shape for the wave pattern, the ellipse perimeter (p) can be calculated from the following formula by Ramanujan:

$$P \approx \pi[3(a + b) - \sqrt{(3a + b)(a + 3b)}]$$

where a and b are the radii of the major and minor axis, respectively.[49] The p value is found to be 453.3 μm, which is about 1.3 times longer than its original length of 350 μm. Hence, the wavy-shaped textured graphene/PDMS film can be stretched to about 130% in a horizontal stretching direction, as schematically shown in Figure 4b.

An important feature of the textured graphene/PDMS film is the high stretching and bending ability of the electrode in any direction. As shown in the schematic (Figure 4c), the as-synthesized textured graphene/PDMS film is highly stretchable and recoverable in all directions. This high stretchability of the textured graphene/PDMS film was visualized by the corresponding photograph and optical images for stretching tests. Figure 5a demonstrates the structural evolution of the textured graphene/PDMS film under different tensile strains (0, 10, 20, and 30%). Interestingly, the concentric circular pattern of the textured graphene/PDMS film can be effectively transformed without any structural defects by delocalizing the applied tensile strains. During stretching, the lateral dimensions of the wavy graphene/PDMS film are expanded until the curved state shifts to a flat one (Figure 5b). The flattened graphene/PDMS film develops a wave pattern when it is relaxed. This process is reversible over multiple cycles under controlled substrate deformation.

Tensile testing was also performed to investigate the mechanical properties of a textured graphene/PDMS film (see the Supporting Information S3). The stress and strain initially increase with a linear relationship up to strain values of 40%. This is the linear-elastic portion of the curve, and it indicates that no plastic deformation has occurred. In this region of the curve, when the stress is reduced, the textured graphene/PDMS film will return to its original shape. Hence, the Young's modulus (E) was calculated for this linear elastic region (under 40% strain) using Hooke's law, and the average E value of the textured graphene/PDMS film was 1.3 MPa, which is fairly close to that of pristine PDMS (1.32 ± 0.07 MPa).[50]

To clearly understand the effects of the textured shape of graphene on the effective stress (σ_{eff}) distribution, a finite element method (FEM) simulation was performed using Midas NFX (Midas IT Co.). Figure 6a shows the 3D FEM models for the flat, 1D wavy, and textured graphene with $x-y$ dimensions of 1 mm × 1 mm. The wavelength of the wavy structures was 350 μm, and their amplitude was 55 μm (which corresponds to the real value from height analysis). Due to the too large wavelength and amplitude compared to the actual thickness (~1 nm) of multilayered graphene, we could not help modeling the graphene with a minimum thickness of 0.5 μm. However, we are sure that our simulation is sufficient to understand the shape effects of graphene in this study even though the thickness of graphene is greatly different. A more detailed thickness effect on the simulation is presented in the

DOI: 10.1021/acsnano.6b04493
ACS Nano 2016, 10, 9446−9455

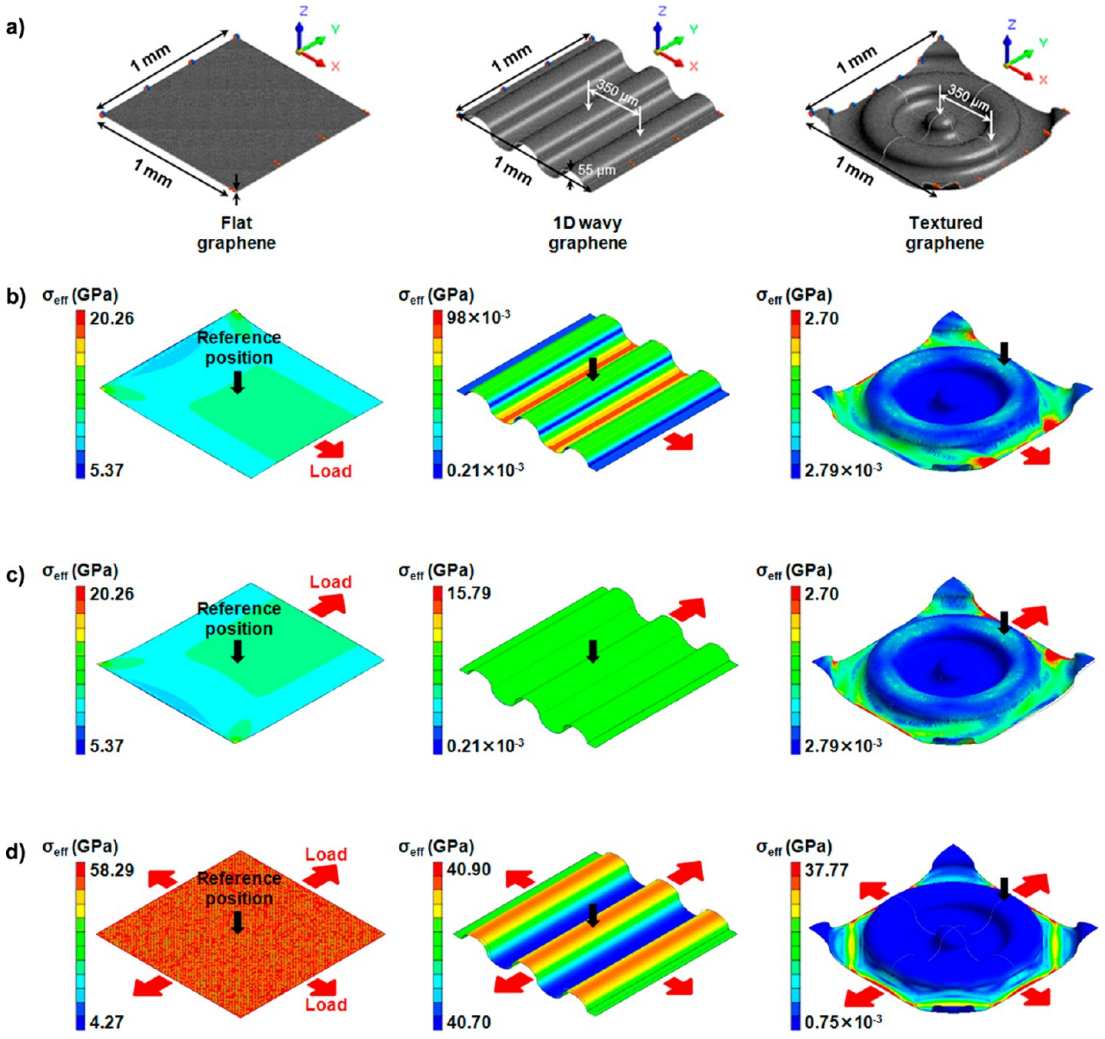

Figure 6. (a) FEM models for flat, one-directional (1D) wavy, and textured graphene. The $x-y$ size was limited to 1 mm × 1 mm. The wavelength and amplitude for 1D and textured graphene were 350 μm and 55 μm from experimentally measured data. (b, c) Stress distributions for flat, 1D wavy, and textured shapes of graphene under a load direction of the (b) x-axis and (c) y-axis. Strain was 1% in the x- and y-axis directions, respectively. The black arrow is the reference position where we select the effective stress on each sample for comparison. (d) Stress distributions under a biaxial load ($x-y$ direction) with 2% strain.

Supporting Information S4. We applied a load with displacement control where the maximum strain was 1% in the x- and y-axis directions under uniaxial load, respectively. For a biaxial load, we applied a 2% strain. Finally, the total effective stresses, σ_{eff}, were calculated using von Mises theory:

$$\sigma_{eff} = \int_V \{\sqrt{\sigma_{11}^2 + \sigma_{22}^2 + \sigma_{33}^2 - \sigma_1\sigma_2 - \sigma_2\sigma_3 - \sigma_1\sigma_3}\}\, dV$$

where V is the entire volume.[51] In order to compare the mechanical strength depending on the graphene shape, we selected the effective stresses at reasonable reference positions (black arrows in Figure 6b, c, and d) on each sample because edge and boundary effects in the calculations should be eliminated. We further discuss these edge and boundary effects in the Supporting Information S5.

When a load is applied along the x-axis (Figure 6b), the graphene with a 1D wavy shape provides an effective stress of about 0.09 GPa, which is about 100 times lower than that of the graphene with a flat shape (11.57 GPa) and about 10 times lower than that of the textured graphene (1.07 GPa). However, the effective stress of the 1D wavy graphene increased to about 100 times (10.90 GPa) when a load is applied along the y-axis (Figure 6c). On the other hand, the textured graphene showed almost the same value (1.06 GPa) of effective stress (see Table 1), which is about 10 times lower than that of 1D graphene. Thus, it can be clearly understood that the effective stress of graphene is critically dependent on the shape. Particularly, the effective stress of a 1D wavy graphene is greatly dependent on the load direction, while that of the textured graphene is not dependent on the load direction.

The films were also subjected to a biaxial load ($x-y$ direction) to further understand the shape effect, as shown in Figure 6d. We compared the effective stresses at the reference positions that were selected in a uniaxial loading condition. Under a biaxial load, a flat graphene showed the same stress distribution (58.3 GPa) at the maximum and minimum values. Similarly, a 1D wavy graphene provided almost the same stress distribution (~40.8 GPa) across the total film, which was about 30% less than that of the flat one. Interestingly, a textured graphene showed about 6 times less effective stress (~9.4 GPa), and particularly most of effective stresses (about 90% on the total film) showed 10^4-fold less values (~10 MPa). Finally, we

DOI: 10.1021/acsnano.6b04493
ACS Nano 2016, 10, 9446−9455

Table 1. Effective Stresses at Each Graphene Structure and Increment Ratio between *y*-Axis Maximum Effective Stress and *x*-Axis Maximum Effective Stress

Sample	FEM models[a]	*x*–axis maximum effective stress[b] (σ_x)	*y*–axis maximum effective stress[b] (σ_y)	Increment ratio (σ_y/σ_x)
Flat graphene	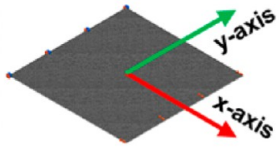	11.57 GPa	11.81 GPa	1.02
1D wavy graphene	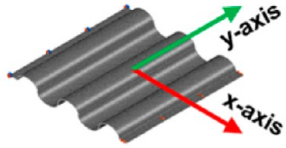	0.09 GPa	10.90 GPa	121.11
Textured graphene	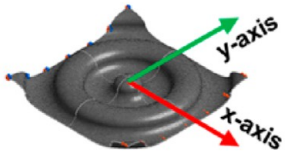	1.07 GPa	1.06 GPa	0.99

[a]The *x*–*y* size was 1 × 1 mm, and the wavelength and amplitude for 1D and textured graphene were 350 and 55 μm. The maximum strain was 1% in the *x*- and *y*-axis directions, respectively. [b]The maximum effective stresses were calculated by using Midas NFX (Midas IT Co.).

can conclude that a textured shape for graphene is greatly useful under omnidirectional loads in terms of mechanical stability.

In order to demonstrate the superiority of a highly stretchable yet mechanically durable textured graphene/PDMS film, the electrical properties of the omnidirectionally stretchable graphene electrodes were measured under various mechanical stresses using a two-point probe method. As depicted in Figure 7a and b, sheet resistances of the graphene/PDMS film were systematically monitored under various bending and stretching conditions. Interestingly, the textured graphene/PDMS film nearly maintains its electrical properties when the film is folded with a bending radius (r) as small as r = 0.5 mm or stretched up to 30% of the tensile strain. The stretching of the textured graphene/PDMS film to 30% of the tensile strain led to about a 0.45-fold increase in resistance, which then returned to close to the original value when the force was removed. More stretching test results over 1000 times are presented in the Supporting Information S6. This stable and reversible change in the resistance can be attributed to the lateral expansion of the wavy pattern configuration, as previously shown in Figure 4c. The textured graphene/PDMS film can be effectively transformed (by bending or stretching) with slight variation in electrical resistance, indicating a much better mechanical stability of the graphene sheets. In contrast, the resistance of the bare graphene on the PDMS film is irreversibly increased by orders of magnitude under similar deformation conditions, owing to the inevitable structural fracture of the graphene sheets.

In order to obtain in-depth insight into the omnidirectional stretchability, the electrical fatigue of the textured graphene/PDMS film under different stretching angles (from 0° to 90°) was measured (inset in Figure 7c). The electrical fatigue was calculated by measuring the sheet resistance change, $\Delta R/R_0 = (R - R_0)/R_0$, where R and R_0 are the measured and initial sheet resistances, respectively. As presented in Figure 7c, when the film is stretched with 30% tensile strain, the textured graphene/PDMS film shows resistance values of 0.946, 1.014, 0.917, and 0.958 kΩ at stretching angles of 0°, 30°, 60°, and 90°, respectively. It is worth noting that the textured graphene/PDMS film possesses an electrical stability and reliability under various stretching directions, and the angular dependence does not significantly influence the electrical properties.

Figure 7d demonstrates the practical applications of a stretchable electrode. An optically transparent and electrically conductive graphene/PDMS film (thickness of PDMS is 2 mm, width is 150 mm) was gently attached to the joint of a finger, and the resistance changes were measured in real time as the finger was bent cyclically. The textured graphene/PDMS film was bent convexly and concavely by the folding and unfolding motions of the finger. Under the folding/unfolding finger motions, the sheet resistances could be reversibly varied from 0.65 kΩ (concave bent) to 0.71 kΩ (convex bent). The average sheet resistance change ($\Delta R/R_0$) is less than 0.09 during different stages of the repeated finger motions.

CONCLUSION

In conclusion, we developed omnidirectionally stretchable and transparent electrodes based on multilayered graphene on a textured elastomeric substrate. The mechanical and electrical properties of the prepared samples were systematically investigated. The textured graphene/PDMS film with concentric circle patterns enables us to achieve a high optical transparency (up to 87% at 550 nm), excellent stretchability (up to 30% of the strain), and good electrical stability.

DOI: 10.1021/acsnano.6b04493
ACS Nano 2016, 10, 9446–9455

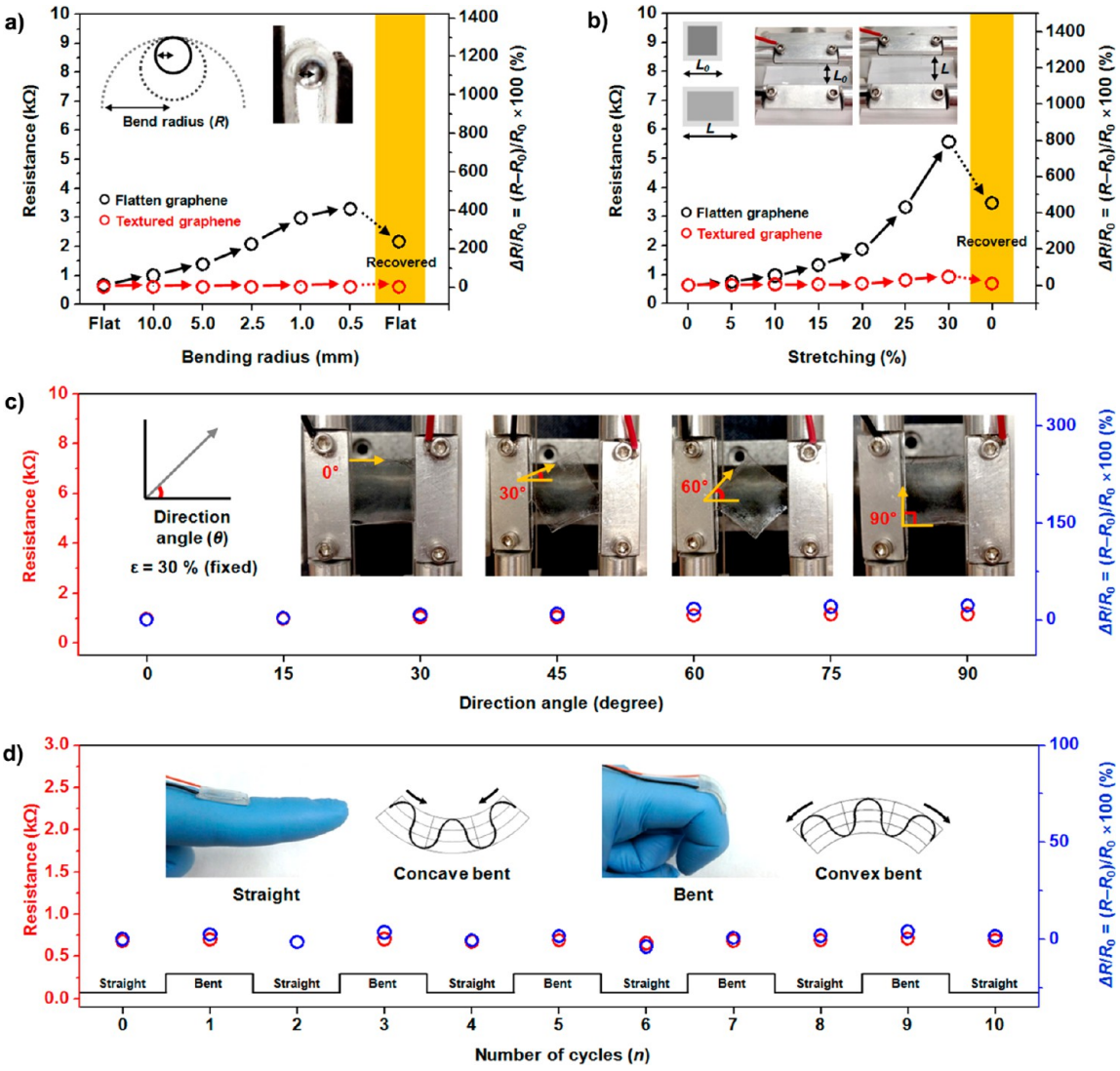

Figure 7. Variation in resistance of a textured graphene/PDMS film as a function of (a) bending radius and (b) tensile strains (insets: actual test images for a graphene/PDMS film). (c) Variation in resistance of a textured graphene/PDMS film under various stretching angles (from 0° to 90°). Stretching tests were performed under a fixed tensile strain of 30%. (d) Variation in resistance of a textured graphene/PDMS film as a function of a finger-bending cycle.

Particularly, the pattern configuration allows effective transformation of the graphene/PDMS film under mechanical stresses without any structural defects by delocalizing the applied tensile strains. The film exhibits reliable electrical performances regardless of the stretching direction, manifesting omnidirectional stretchability. This study can be significant for a large variety of potential applications, ranging from stretchable devices to electronic components in various wearable integrated systems.

METHODS

Synthesis of Multilayered Graphene. Multilayered graphene was grown by a typical atmospheric pressure chemical vapor deposition. Briefly, the 25 μm thick Cu foil (99.8%, Alfa Aesar) was prepatterned by pressing it with a Fresnel lens, which acted as a mold. The prepatterned Cu foil was loaded into a CVD chamber. To reduce the native copper oxide and to facilitate Cu grain growth, the prepatterned Cu foil was annealed at CVD temperature for 30 min in a flow of argon (Ar, 1000 sccm) and hydrogen (H_2, 300 sccm). After the annealing step, a flow of methane (CH_4, 30 sccm) was introduced to initiate the graphene growth, for 30 min. The graphene growth was carried out at 1000 °C. Once the graphene growth was finished, the CVD chamber was cooled rapidly under 1000 sccm of Ar to prevent oxidation and to minimize hydrogenation reactions of the graphene.

Fabrication of the Textured Graphene/PDMS Film. After graphene growth, a PDMS solution (Sylgard 184, Dow Corning) was spin-coated onto the top side of the sample at 150 rpm for 300 s and thermally cured for 60 min in an oven held at 80 °C. Before the Cu etching process, the back-side graphene was removed by oxygen plasma etching for 3 min at a plasma power of 100 W. Copper etchant (CE-100, Transene Company Inc.) was used to etch the Cu foil, and the textured graphene/PDMS film was floated on the surface of the solution. The textured graphene/PDMS film was moved to distilled water several times to rinse the etchant residue. After rinsing with distilled water, the textured graphene/PDMS film was scooped out and carefully flipped over. Then, the sample was dried in an oven at 60 °C for several hours to enable the complete evaporation of moisture from the sample.

Characterizations. The morphology was confirmed using an optical microscope (Zeiss Primo Star, Carl Zeiss). The surface profile was taken by using a P-16 surface profilometer (KLA-Tencor). The textured graphene/PDMS film was measured for optical transparency with ultraviolet−visible (UV−vis) spectroscopy. The UV−vis spectra

DOI: 10.1021/acsnano.6b04493
ACS Nano 2016, 10, 9446−9455

were taken with a PerkinElmer Lamda 20 spectrometer at a resolution of 1 nm. The Raman measurement was carried out using a Horiba-Jobin Yvon system with a 532 nm Ar+ laser line. The laser power used is around 1 mW on the sample, and a 100× objective was used to focus the beam. The size of the laser beam on the sample was around 1 μm. Tensile tests were performed in an Instron 5848 microtester (Instron Corporation, Canton, MA, USA). The bending and stretching tests were performed using a homemade bending machine with a bending radius of 0.5−10 mm and up to 30% tensile strain. The electrical conductivity was measured by the two-probe method using a Keithley 2400 sourcemeter at room temperature. The mechanical simulation was constructed and calculated by using Midas NFX (Midas IT co.), commercially available FEM software.

ASSOCIATED CONTENT

Supporting Information

The Supporting Information is available free of charge on the ACS Publications website at DOI: 10.1021/acsnano.6b04493.

(1) Influence of high-temperature CVD process on prepattered Cu foil morphology; (2) prepatterned Cu foils with various shapes and configurations; (3) mechanical property of the textured graphene/PDMS film; (4) thickness effects in the simulations; (5) reference position selection in the simulations; and (6) mechanical durability of the textured graphene/PDMS film (PDF)

AUTHOR INFORMATION

Corresponding Authors

*Phone (J. Kong): +1-6173244068. Fax: +1-6173245293. E-mail: jingkong@mit.edu.

*Phone (H. S. Park): +82-312994706. Fax: +82-312907272. E-mail: phs0727@skku.edu.

Notes

The authors declare no competing financial interest.

ACKNOWLEDGMENTS

We would like to acknowledge the financial support from the R&D Convergence Program (CAP-15-02-KBSI) of NST (National Research Council of Science & Technology) and a grant from R&D Program of the Korea Railroad Research Institute (PK1607B) of Republic of Korea, the AFOSR FATE MURI, Grant No. FA9550-15-1-0514, and the STC Center for Integrated Quantum Materials (CIQM) from NSF (US) grant DMR-1231319.

REFERENCES

(1) Yu, Z.; Niu, X.; Liu, Z.; Pei, Q. Intrinsically Stretchable Polymer Light-Emitting Devices Using Carbon Nanotube-Polymer Composite Electrodes. *Adv. Mater.* **2011**, *23*, 3989−3994.

(2) Kim, J. B.; Kim, P.; Pégard, N. C.; Oh, S.; Ju; Kagan, C. R.; Fleischer, J. W.; Stone, H. A.; Loo, Y.- L. Ultrathin, Highly Flexible and Stretchable PLEDs. *Nat. Photonics* **2012**, *6*, 327−332.

(3) Shin, G.; Yoon, C. H.; Bae, M. Y.; Kim, Y. C.; Hong, S. K.; Rogers, J. A.; Ha, J. S. Stretchable Field-Effect-Transistor Array of Suspended SnO_2 Nanowires. *Small* **2011**, *7*, 1181−1185.

(4) Roh, E.; Hwang, B.-U.; Kim, D.; Kim, B.-Y.; Lee, N.-E. Stretchable, Transparent, Ultrasensitive, and Patchable Strain Sensor for Human−Machine Interfaces Comprising a Nanohybrid of Carbon Nanotubes and Conductive Elastomers. *ACS Nano* **2015**, *9*, 6252−6261.

(5) Li, P.; Sun, K.; Ouyang, J. Stretchable and Conductive Polymer Films Prepared by Solution Blending. *ACS Appl. Mater. Interfaces* **2015**, *7*, 18415−18423.

(6) Stoyanov, H.; Kollosche, M.; Risse, S.; Waché, R.; Kofod, G. Soft Conductive Elastomer Materials for Stretchable Electronics and Voltage Controlled Artificial Muscles. *Adv. Mater.* **2013**, *25*, 578−583.

(7) Chen, T.; Peng, H. S.; Durstock, M.; Dai, L. M. High-Performance Transparent and Stretchable All-Solid Supercapacitors Based on Highly Aligned Carbon Nanotube Sheets. *Sci. Rep.* **2014**, *4*, 3612.

(8) Ginga, N. J.; Chen, W.; Sitaraman, S. K. Waviness Reduces Effective Modulus of Carbon Nanotube Forests by Several Orders of Magnitude. *Carbon* **2014**, *66*, 57−66.

(9) Won, Y.; Gao, Y.; Panzer, M. A.; Xiang, R.; Maruyama, S.; Kenny, T. M.; Cai, W.; Goodson, K. E. Zipping, Entanglement, and the Elastic Modulus of Aligned Single-Walled Carbon Nanotube Films. *Proc. Natl. Acad. Sci. U. S. A.* **2013**, *110*, 20426−20430.

(10) Hu, L.; Pasta, M.; Mantia, F. L.; Cui, L.; Jeong, S.; Deshazer, H. D.; Choi, J. W.; Han, S. M.; Cui, Y. Stretchable, Porous, and Conductive Energy Textiles. *Nano Lett.* **2010**, *10*, 708−714.

(11) Jost, K.; Perez, C. R.; McDonough, J. K.; Presser, V.; Heon, M.; Dion, G.; Gogotsi, Y. Carbon Coated Textiles for Flexible Energy Storage. *Energy Environ. Sci.* **2011**, *4*, 5060−5067.

(12) Hu, W.; Niu, X.; Li, L.; Yun, S.; Yu, Z.; Pei, Q. Intrinsically Stretchable Transparent Electrodes Based on Silver-Nanowire−Crosslinked-Polyacrylate Composites. *Nanotechnology* **2012**, *23*, 344002.

(13) Hyun, D. C.; Park, M.; Park, C.; Kim, B.; Xia, Y.; Hur, J. H.; Kim, J. M.; Park, J. J.; Jeong, U. Ordered Zigzag Stripes of Polymer Gel/Metal Nanoparticle Composites for Highly Stretchable Conductive Electrodes. *Adv. Mater.* **2011**, *23*, 2946−2950.

(14) Kim, D.-H.; Xiao, J.; Song, J.; Huang, Y.; Rogers, J. A. Stretchable, Curvilinear Electronics Based on Inorganic Materials. *Adv. Mater.* **2010**, *22*, 2108−2124.

(15) Park, M.; Im, J.; Shin, M.; Min, Y.; Park, J.; Cho, H.; Park, S.; Shim, M.-B.; Jeon, S.; Chung, D.-Y.; Bae, J.; Park, J.; Jeong, U.; Kim, K. Highly Stretchable Electric Circuits from a Composite Material of Silver Nanoparticles and Elastomeric Fibres. *Nat. Nanotechnol.* **2012**, *7*, 803−809.

(16) Lee, J.; Wu, J.; Shi, M. X.; Yoon, J.; Park, S. I.; Li, M.; Liu, Z. J.; Huang, Y. G.; Rogers, J. A. Stretchable GaAs Photovoltaics with Designs That Enable High Areal Coverage. *Adv. Mater.* **2011**, *23*, 986−991.

(17) Park, S.-I.; Xiong, Y.; Kim, R.-H.; Elvikis, P.; Meitl, M.; Kim, D.-H.; Wu, J.; Yoon, J.; Yu, C.-J.; Liu, Z.; Huang, Y.; Hwang, K.-C.; Ferreira, P.; Li, X.; Choquette, K.; Rogers, J. A. Printed Assemblies of Inorganic Light-Emitting Diodes for Deformable and Semitransparent Displays. *Science* **2009**, *325*, 977−981.

(18) Yu, C.; Masarapu, C.; Rong, J.; Wei, B.; Jiang, H. Stretchable Supercapacitors Based on Buckled Single-Walled Carbon-Nanotube Macrofilms. *Adv. Mater.* **2009**, *21*, 4793−4797.

(19) Niu, Z.; Dong, H.; Zhu, B.; Li, J.; Hng, H. H.; Zhou, W.; Chen, X.; Xie, S. Highly Stretchable, Integrated Supercapacitors Based on Single-Walled Carbon Nanotube Films with Continuous Reticulate Architecture. *Adv. Mater.* **2013**, *25*, 1058−1064.

(20) Xu, F.; Wang, X.; Zhu, Y.; Zhu, Y. Wavy Ribbons of Carbon Nanotubes for Stretchable Conductors. *Adv. Funct. Mater.* **2012**, *22*, 1279−1283.

(21) Khang, D.-Y.; Xiao, J.; Kocabas, C.; MacLaren, S.; Banks, T.; Jiang, H.; Huang, Y. Y.; Rogers, J. A. Molecular Scale Buckling Mechanics in Individual Aligned Single-Wall Carbon Nanotubes on Elastomeric Substrates. *Nano Lett.* **2008**, *08*, 124−130.

(22) Shin, K.-Y.; Hong, J.-Y.; Jang, J. Micropatterning of Graphene Sheets by Inkjet Printing and Its Wideband Dipole-Antenna Application. *Adv. Mater.* **2011**, *23*, 2113−2118.

(23) Hong, J.-Y.; Shin, K.-Y.; Kwon, O. S.; Kang, H.; Jang, J. A Strategy for Fabricating Single Layer Graphene Sheets Based on a Layer-by-Layer Self-Assembly. *Chem. Commun.* **2011**, *47*, 7182−7184.

(24) Shin, K.-Y.; Hong, J.-Y.; Jang, J. Flexible and Transparent Graphene Films as Acoustic Actuator Electrodes Using Inkjet Printing. *Chem. Commun.* **2011**, *47*, 8527−8529.

DOI: 10.1021/acsnano.6b04493
ACS Nano 2016, 10, 9446−9455

(25) Hong, J.-Y.; Jang, J. Micropatterning of Graphene Sheets: Recent Advances in Techniques and Applications. *J. Mater. Chem.* **2012**, *22*, 8179−8191.
(26) Hong, J.-Y.; Kong, J.; Kim, S. H. Spatially Controlled Graphitization of Reduced Graphene Oxide Films *via* a Green Mechanical Approach. *Small* **2014**, *10*, 4839−4844.
(27) Xu, P.; Kang, J.; Choi, J.-B.; Suhr, J.; Yu, J.; Li, F.; Byun, J.-H.; Kim, B.-S.; Chou, T.-W. Laminated Ultrathin Chemical Vapor Deposition Graphene Films Based Stretchable and Transparent High-Rate Supercapacitor. *ACS Nano* **2014**, *8*, 9437−9445.
(28) Chen, T.; Xue, Y.; Roy, A. K.; Dai, L. Transparent and Stretchable High-Performance Supercapacitors Based on Wrinkled Graphene Electrodes. *ACS Nano* **2013**, *8*, 1039−1046.
(29) Zang, J.; Ryu, S.; Pugno, N.; Wang, Q.; Tu, Q.; Buehler, M. J.; Zhao, X. Multifunctionality and Control of the Crumpling and Unfolding of Large-Area Graphene. *Nat. Mater.* **2013**, *12*, 321−325.
(30) Xie, Y.; Liu, Y.; Zhao, Y.; Tsang, Y. H.; Lau, S. P.; Huang, H.; Chai, Y. Stretchable All-Solid-State Supercapacitor with Wavy Shaped Polyaniline/Graphene Electrode. *J. Mater. Chem. A* **2014**, *2*, 9142−9149.
(31) Nam, I.; Bae, S.; Park, S.; Yoo, Y. G.; Lee, J. M.; Han, J. W.; Yi, J. Omnidirectionally Stretchable, High Performance Supercapacitors Based on a Graphene−Carbon-Nanotube Layered Structure. *Nano Energy* **2015**, *15*, 33−42.
(32) Won, S.; Hwangbo, Y.; Lee, S.-K.; Kim, K.-S.; Kim, K.-S.; Lee, S.-M.; Lee, H.-J.; Ahn, J.-H.; Kim, J.-H.; Lee, S.-B. Double-Layer CVD Graphene as Stretchable Transparent Electrodes. *Nanoscale* **2014**, *6*, 6057−6064.
(33) Kim, K. S.; Zhao, Y.; Jang, H.; Lee, S. Y.; Kim, J. M.; Kim, K. S.; Ahn, J.-H.; Kim, P.; Choi, J.-Y.; Hong, B. H. Large-Scale Pattern Growth of Graphene Films for Stretchable Transparent Electrodes. *Nature* **2009**, *457*, 706−710.
(34) Reina, A.; Jia, X.; Ho, J.; Nezich, D.; Son, H.; Bulovic, V.; Dresselhaus, M. S.; Kong, J. Large Area, Few-Layer Graphene Films on Arbitrary Substrates by Chemical Vapor Deposition. *Nano Lett.* **2009**, *9*, 30−35.
(35) Nguyen, V. T.; Le, H. D.; Nguyen, V. C.; Ngo, T. T. T.; Le, D. Q.; Nguyen, X. N.; Phan, N. M. Synthesis of Multi-Layer Graphene Films on Copper Tape by Atmospheric Pressure Chemical Vapor Deposition Method. *Adv. Nat. Sci.: Nanosci. Nanotechnol.* **2013**, *4*, 035012.
(36) Wang, H.; Wang, G.; Bao, P.; Yang, S.; Zhu, W.; Xie, X.; Zhang, W.-J. Controllable Synthesis of Submillimeter Single-Crystal Monolayer Graphene Domains on Copper Foils by Suppressing Nucleation. *J. Am. Chem. Soc.* **2012**, *134*, 3627−3630.
(37) Gan, L.; Luo, Z. Turning off Hydrogen To Realize Seeded Growth of Subcentimeter Single-Crystal Graphene Grains on Copper. *ACS Nano* **2013**, *7*, 9480−9488.
(38) Ibrahim, A.; Akhtar, S.; Atieh, M.; Karnik, R.; Laoui, T. Effects of Annealing on Copper Substrate Surface Morphology and Graphene Growth by Chemical Vapor Deposition. *Carbon* **2015**, *94*, 369−377.
(39) Ferrari, A. C.; Meyer, J. C.; Scardaci, V.; Casiraghi, C.; Lazzeri, M.; Mauri, F.; Piscanec, S.; Jiang, D.; Novoselov, K. S.; Roth, S.; Geim, A. K. Raman Spectrum of Graphene and Graphene Layers. *Phys. Rev. Lett.* **2006**, *97*, 187401.
(40) Hao, Y.; Wang, Y.; Wang, L.; Ni, Z.; Wang, Z.; Wang, R.; Koo, C. K.; Shen, Z.; Thong, J. T. L. Probing Layer Number and Stacking Order of Few-Layer Graphene by Raman Spectroscopy. *Small* **2010**, *6*, 195−200.
(41) Lui, C. H.; Li, Z.; Chen, Z.; Klimov, P. V.; Brus, L. E.; Heinz, T. F. Imaging Stacking Order in Few-Layer Graphene. *Nano Lett.* **2011**, *11*, 164−169.
(42) Wang, Y. Y.; Ni, Z. H.; Shen, Z. X.; Wang, H. M.; Wu, Y. H. Interference Enhancement of Raman Signal of Graphene. *Appl. Phys. Lett.* **2008**, *92*, 043121.
(43) Graf, D.; Molitor, F.; Ensslin, K.; Stampfer, C.; Jungen, A.; Hierold, C.; Wirtz, L. Spatially Resolved Raman Spectroscopy of Single- and Few-Layer Graphene. *Nano Lett.* **2007**, *7*, 238−242.
(44) Nair, R. R.; Blake, P.; Grigorenko, A. N.; Novoselov, K. S.; Booth, T. J.; Stauber, T.; Peres, N. M. R.; Geim, A. K. Fine Structure Constant Defines Visual Transparency of Graphene. *Science* **2008**, *320*, 1308.
(45) Mak, K. F.; Sfeir, M. Y.; Wu, Y.; Lui, C. H.; Misewich, J. A.; Heinz, T. F. Measurement of the Optical Conductivity of Graphene. *Phys. Rev. Lett.* **2008**, *101*, 196405.
(46) Xiao, Y. M.; Xu, W.; Zhang, Y. Y.; Peeters, F. M. Optoelectronic Properties of ABC-Stacked Trilayer Graphene. *Phys. Status Solidi B* **2013**, *250*, 86−94.
(47) Kim, P.; Hu, Y.; Alvarenga, J.; Kolle, M.; Suo, Z.; Aizenberg, J. Rational Design of Mechano-Responsive Optical Materials by Fine Tuning the Evolution of Strain-Dependent Wrinkling Patterns. *Adv. Opt. Mater.* **2013**, *1*, 381−388.
(48) Kang, P.; Wang, M. C.; Knapp, P. M.; Nam, S. W. Crumpled Graphene Photodetector with Enhanced, Strain-Tunable, and Wavelength-Selective Photoresponsivity. *Adv. Mater.* **2016**, *28*, 4639−4645.
(49) Chung, D. D.; Wolfgramm, R. Maxillary Arch Perimeter Prediction Using Ramanujan's Equation for the Ellipse. *Am. J. Orthod.* **2015**, *147*, 235−241.
(50) Johnston, I. D.; McCluskey, D. K.; Tan, C. K. L.; Tracey, M. C. Mechanical Characterization of Bulk Sylgard 184 for Microfluidics and Microengineering. *J. Micromech. Microeng.* **2014**, *24*, 035017.
(51) Mises, R. V. Mechanics of Solid Bodies in the Plastically-Deformable State. *Nachr. Math. Phys.* **1913**, *1*, 582−592.

DOI: 10.1021/acsnano.6b04493
ACS Nano 2016, 10, 9446−9455